

# Energy- and Time-Dependent Branching to Competing Paths in Coupled Unimolecular Dissociations of Chlorotoluene Radical Cations<sup>†</sup>

Jongcheol Seo,<sup>‡</sup> Seung Joon Kim,<sup>§</sup> and Seung Koo Shin<sup>\*,\*</sup>

<sup>‡</sup>Department of Chemistry, Pohang University of Science and Technology, Pohang 790-784, Korea

\*E-mail: skshin@postech.ac.kr

<sup>§</sup>Department of Chemistry, Hannam University, Daejeon 300-791, Korea

Received September 25, 2013, Accepted October 13, 2013

The energy- and time-dependent branching to the competing dissociation paths are studied by theory for coupled unimolecular dissociations of the *o*-, *m*-, and *p*-chlorotoluene radical cations to C<sub>7</sub>H<sub>7</sub><sup>+</sup> (benzylum and tropylium). There are four different paths to C<sub>7</sub>H<sub>7</sub><sup>+</sup>, three to the benzylum ion and one to the tropylium ion, and all of them are coupled together. The branching to the multiple paths leads to the multiexponential decay of reactant with the branching ratio depending on both internal energy and time. To gain insights into the multipath branching, we study the detailed kinetics as a function of time and internal energy on the basis of ab initio/RRKM calculations. The number of reaction steps to C<sub>7</sub>H<sub>7</sub><sup>+</sup> is counted for each path. Of the three isomers, the *meta* mostly goes through the coupling, whereas the *para* proceeds with little or no coupling. In the beginning, some reactants with high internal energy decay fast to the benzylum ion without any coupling and others rearrange to the other isomers. Later on all three isomers dissociate to the products *via* long-lived intermediates. Thus, the reactant shows a multiexponential decay and the branching ratio varies with time as the average internal energy decreases with time. The reciprocal of the effective lifetime is taken as the rate constant. The resulting rate-energy curves are in line with experiments. The present results suggest that the coupling between the stable isomers is thermodynamically controlled, whereas the branching to the product is kinetically controlled.

**Key Words** : Chlorotoluene radical cation, Unimolecular dissociation, Coupled reaction

## Introduction

The unimolecular dissociation of halotoluene radical cations (C<sub>7</sub>H<sub>7</sub>X<sup>+</sup>) has attracted much interest because the radical cations undergo complex hydrogen atom and methylene migrations before C–X cleavage to the product ion C<sub>7</sub>H<sub>7</sub><sup>+</sup> (benzylum and tropylium). Both experiments<sup>1–8</sup> and theory<sup>9–13</sup> have shown that the benzylum ion is kinetically favored over the thermodynamically more stable tropylium ion.

In the present work, we studied the energy- and time-dependent branching of the *o*-, *m*-, and *p*-chlorotoluene radical cations to the two competing products in order to understand the details of dissociation kinetics as a function of internal energy. Of the halotoluenes, chlorotoluene was chosen because recent density functional theory (DFT) calculations suggested that all three isomers were interconnected through hydrogen and methylene migrations on the ring below the dissociation barrier.<sup>12</sup> We have previously reported the kinetics of the multiple-barrier unimolecular dissociation of the chlorotoluene radical cation on the basis of the potential energy surface provided by the SCF method.<sup>11</sup> No coupling between isomers was considered because the two product ions were thought to be originated from the two separate paths involving [1,3] and [1,2]  $\alpha$ -H migrations from

the reactant. However, the recent study with the density functional theory (DFT) have indicated that the [1,2]  $\alpha$ -H migration is the first step of the complex rearrangement processes and the direct [1,3]  $\alpha$ -H migration is not necessary for the formation of the benzylum ion.<sup>13</sup> In theoretical studies of the kinetics of coupled unimolecular dissociations of the bromotoluene radical cations, we have found that the product branching ratio is time-dependent because of the coupling and the decay of reactant is not single exponential.<sup>13</sup> Moreover, the coupled unimolecular dissociation cannot be assumed as a single-barrier process and the steady-state approximation cannot be applied to describe the kinetics of the coupled dissociations. Thus, in the present study, we revisited the unimolecular dissociations of the chlorotoluene radical cations with the coupling scheme shown in Figure 1 to characterize the energy- and time-dependent branching to the competing dissociation paths.

The mechanism including all elementary steps is depicted in Figure S1 (See Supplementary Material). The dissociation reaction begins with the [1,2]  $\alpha$ -H migration of **1-x** to **2-x** ( $x = o, m, \text{ and } p$ ).<sup>13</sup> From the intermediate **2-x**, the dissociation path is split either to the benzylum ion or to the tropylium ion. The ring expansion from **4-x** to **5-x** followed by H-atom migrations on the 7-membered ring yields **6** that leads to the tropylium ion with a loss of chlorine. The C–X cleavage from **6** is the only exit channel to the tropylium ion, which is denoted **6**  $\rightarrow$  Tr<sup>+</sup>. On the other hand, the H-atom migration

<sup>†</sup>This paper is to commemorate Professor Myung Soo Kim's honourable retirement.

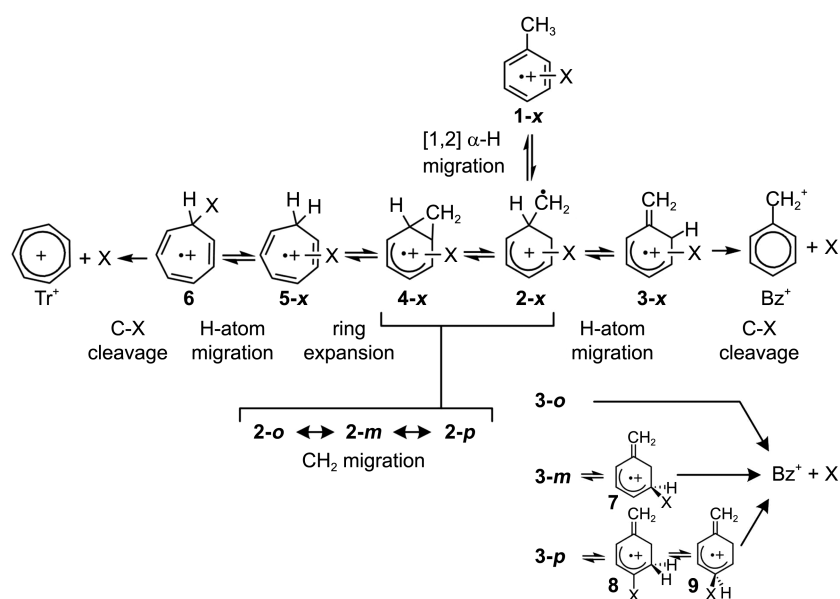


**Figure 1.** Complex rearrangements of the chlorotoluene ( $X = \text{Cl}$ ) radical cation,  $1-x$  ( $x = o, m,$  and  $p$ ), prior to its dissociation either to the benzylium ion ( $\text{Bz}^+$ ) or to the tropylium ion ( $\text{Tr}^+$ ).

on the 6-membered ring converts  $2-x$  to  $3-x$  that proceeds to the production of the benzylium ion. In fact, the *o*-, *m*-, and *p*-isomers yield the benzylium ion through the three different exit channels:  $3-o \rightarrow \text{Bz}^+$ ,  $7 \rightarrow \text{Bz}^+$ , and  $9 \rightarrow \text{Bz}^+$ . Importantly,  $2-o$ ,  $2-m$ , and  $2-p$  are interconnected *via*  $4-x$ . The  $\text{CH}_2$  migration on the six-membered ring can convert  $2-o$  into  $2-m$ ,  $2-m$  into either  $2-o$  or  $2-p$ , and  $2-p$  into  $2-m$ . Thus, there are four dissociation paths that are coupled together regardless of the initial reactant.

With this coupled reaction scheme of the *o*-, *m*-, and *p*-chlorotoluene radical cations, we investigated the details of the product branching to the competing dissociation paths by using *ab initio*/RRKM calculations. The extent of the coupling between *o*-, *m*-, and *p*-isomers is investigated as a function of the internal energy by calculating the relative abundances of the product ions generated through four different exit channels:  $6 \rightarrow \text{Tr}^+$  to the tropylium ion and  $3-o \rightarrow \text{Bz}^+$ ,  $7 \rightarrow \text{Bz}^+$ , and  $9 \rightarrow \text{Bz}^+$  to the benzylium ion. The number of steps taken to each exit channel is simulated and temporal variations of the reactant and the transient isomers  $1-x$  ( $x = o, m,$  and  $p$ ) are simulated. Taken these results together, we discussed the energy- and time-dependent characteristics of the branching to the coupled dissociation paths in this complex multi-barrier unimolecular dissociation.

### Computational Details

The geometries of the local minima and transition states were optimized using DFT with the Becke three-parameter Lee–Yang–Parr (B3LYP) functional and the augmented correlation-consistent polarized valence-only double-zeta (aug-cc-pVDZ) basis set using a Gaussian-03 program.<sup>14</sup> The relative energies, harmonic vibrational frequencies, and rotational constants of all transient species were obtained at the same level of theory for the RRKM calculation. The

harmonic vibration frequencies were scaled by 0.97.<sup>15</sup> The RRKM calculation was performed by using a homemade program. The microcanonical rate constants of all elementary steps were calculated using the RRKM equation, as given in Eq. (1).<sup>16</sup>

$$k(E) = \frac{\sigma W^\ddagger(E - E_0 - E_r^\ddagger)}{h \rho(E - E_r)} \quad (1)$$

$E$  is the internal energy of a radical cation and  $E_0$  is the threshold energy.  $E_r$  and  $E_r^\ddagger$  are the rotational energies of the reactant and transition state, respectively. The external rotation is treated adiabatically.  $\sigma$  is the reaction degeneracy.  $W^\ddagger$  is the sum of vibrational states of the transition state and  $\rho$  is the density of vibrational states of the reactant. The sum and density of states were counted using a Beyer–Swinehart direct counting algorithm.<sup>16</sup>

Temporal variations of all the transient species, including three reactants ( $1-x$ ) and 16 intermediates, were examined by numerically solving the 19 rate equations using the matrix formulation.<sup>11,13</sup> The relative abundances of product ions through four exit channels were numerically traced by integrating the rate equations for the exit channels at given internal energy  $E$  until their sum reached 0.999. The detailed calculation procedures have been described elsewhere.<sup>11,13</sup> The decay of the total  $\text{C}_7\text{H}_7\text{Cl}^+$  population was fit to a multiexponential function as given in Eq. (2). The inverse of the effective decay time constant  $\tau_{\text{eff}}^{-1}$  ( $\tau_{\text{eff}}^{-1} = c_1 \tau_1^{-1} + c_2 \tau_2^{-1} + c_3 \tau_3^{-1}$ ) is considered as the microcanonical rate constant  $k_{\text{uni}}(E)$  for the overall dissociation reaction.

$$f(t) = c_1 e^{-t/\tau_1} + c_2 e^{-t/\tau_2} + c_3 e^{-t/\tau_3} \quad (2)$$

The number of elementary steps to the product was counted by Monte-Carlo method. For the step counting, the internal energy of the initial reactant was set at 2.5 eV, the

RRKM rate constants were calculated for all elementary steps, and the probability for all transient species moving one step was calculated in every 100 ps. Then, the reactant  $1-x$  moved to the next step every 100 ps until it passed through the final step toward either the benzylium ion or the tropylium ion. The total number of elementary steps to reach the product was counted for all four exit channels ( $3-o \rightarrow Bz^+$ ,  $7 \rightarrow Bz^+$ ,  $9 \rightarrow Bz^+$ , or  $6 \rightarrow Tr^+$ ). Simulation was repeated 100,000 times for each reactant and the probability distribution function for the number of steps was calculated for each exit channel.

## Results

The potential energy surface is shown in Figure 2(a)-(c) for the *o*-, *m*-, and *p*-chlorotoluene radical cations, respectively. The relative energy is listed in Table S1 (See Supplementary Material). The energy levels of  $1-o$  and  $1-m$  are degenerate.  $1-p$  is 3 kcal mol<sup>-1</sup> more stable than the other two isomers. The energy level of  $Tr^+ + Cl$  lies 26, 26, and 29 kcal mol<sup>-1</sup> above  $1-o$ ,  $1-m$ , and  $1-p$ , respectively.  $Tr^+$  is 8 kcal mol<sup>-1</sup> more stable than  $Bz^+$ . The first step of dissociation involves the 1,2 H-atom migration from the methyl group to the ipso carbon. The barrier height for this transition from  $1-x$  to  $2-x$  is 38, 41, and 40 kcal mol<sup>-1</sup> for the *o*-, *m*-, and *p*-isomers, respectively. The relative energy level of  $2-x$  with respect to  $1-x$  is in the order of *meta* > *ortho* > *para*. Of the

intermediates,  $2-x$  is least stable and it branches to two product channels, the benzylium channel *via*  $3-x$  and the tropylium channel *via*  $4-x$ . The  $2-x \rightarrow 3-x$  rearrangement is the highest barrier process along the benzylium channel for all three isomers, whereas the  $2-x \rightarrow 4-x$  process is not the highest barrier one along the tropylium channel because it subsequently involves even higher barrier H-atom migrations on the 7-membered ring ( $5-p \rightarrow 5-m \rightarrow 5-o \rightarrow 6$ ). Thus, the barrier to the benzylium channel is less than that to the tropylium channel for all three isomers. Notably, both  $2-x$  and  $4-x$  play important roles in interconnecting the three isomers: the *o*-isomer is converted to the *m*-isomer through  $2-o \rightarrow 4-m$ , the *m*-isomer is transformed either to the *o*-isomer through  $4-m \rightarrow 2-o$  or to the *p*-isomer through the  $2-m \rightarrow 4-p$ , and the *p*-isomer is rearranged to the *m*-isomer through  $4-p \rightarrow 2-m$ . The barrier height for  $2-o \rightarrow 4-m$  is almost identical to that for  $2-o \rightarrow 4-o$ , indicating that the *o*-isomer can be converted to the *m*-isomer. The barrier height for  $4-m \rightarrow 2-o$  is 5 kcal mol<sup>-1</sup> less than that for  $4-m \rightarrow 2-m$ , and that for  $2-m \rightarrow 4-p$  is 1 kcal mol<sup>-1</sup> less than that for  $2-m \rightarrow 4-m$ . Thus, the *m*-isomer can be readily rearranged to the other two isomers. However, the barrier height for  $4-p \rightarrow 2-m$  is 18 kcal mol<sup>-1</sup>, which is 6 kcal mol<sup>-1</sup> higher than that for  $4-p \rightarrow 2-p$ , suggesting that the *p*-isomer can hardly be converted to the *m*-isomer as well as to the *o*-isomer.

To understand the effects of coupling on the dissociation paths, we examined the relative abundance of the product

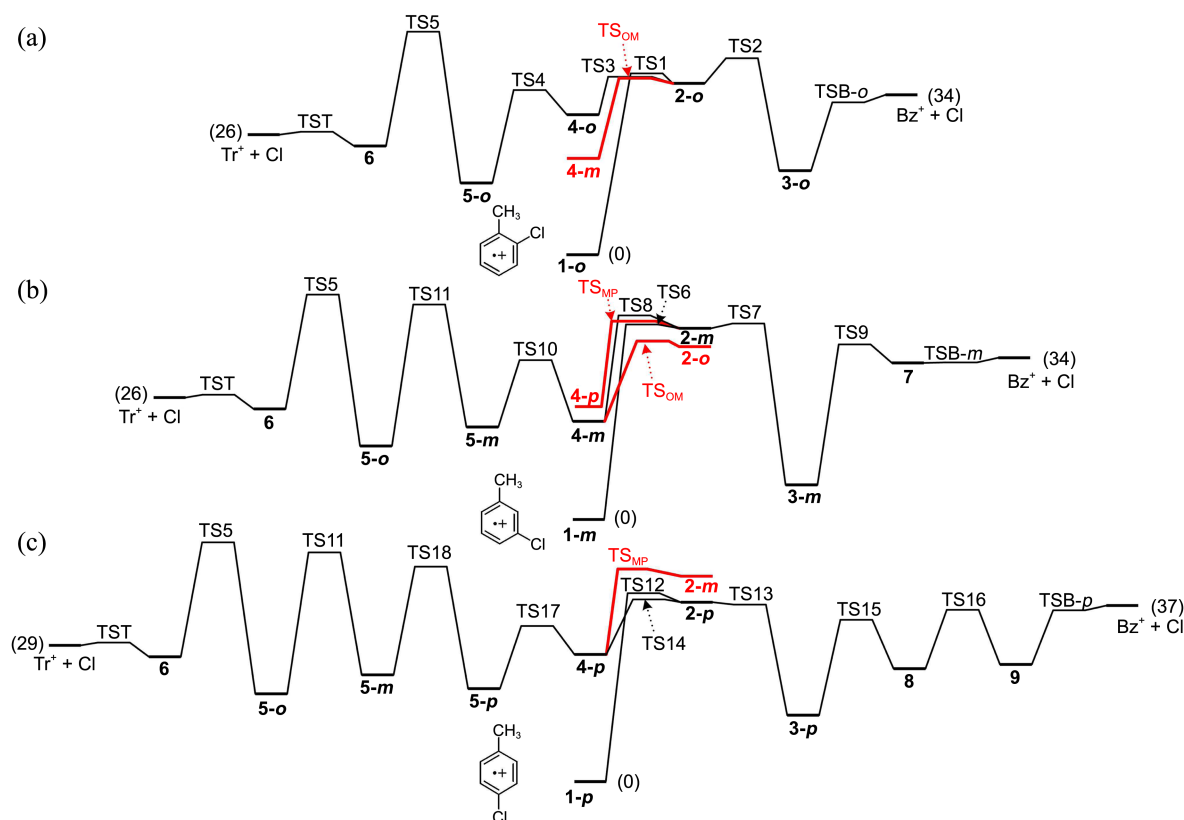


**Figure 2.** The potential energy surface for the unimolecular dissociation of (a) *o*-, (b) *m*-, and (c) *p*-chlorotoluene radical cations. The energy of the local minima and transition states is relative to the reactant  $1-x$  for each *o*-, *m*-, and *p*-isomer. The potential energy surface for the  $CH_2$  migration that interconnects *o*-, *m*-, and *p*-isomers is shown red ( $4-o \leftrightarrow 2-o \leftrightarrow 4-m \leftrightarrow 2-m \leftrightarrow 4-p \leftrightarrow 2-p$ ). The relative energy corrected for the zero-point energy is given in parenthesis in units of kcal mol<sup>-1</sup>.

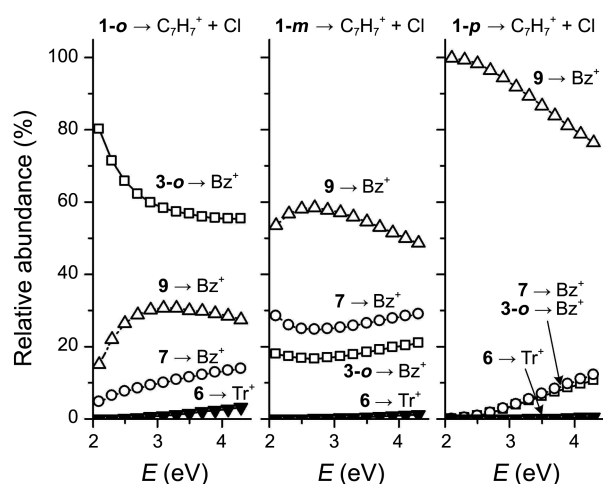


**Figure 3.** The relative abundance of the product from four different exit channels ( $3\text{-}o \rightarrow \text{Bz}^+$ ,  $7 \rightarrow \text{Bz}^+$ ,  $9 \rightarrow \text{Bz}^+$ ,  $6 \rightarrow \text{Tr}^+$ ) for each reactant,  $1\text{-}o$ ,  $1\text{-}m$ , and  $1\text{-}p$ .

ion from the four different exit channels ( $3\text{-}o \rightarrow \text{Bz}^+$ ,  $7 \rightarrow \text{Bz}^+$ ,  $9 \rightarrow \text{Bz}^+$ , and  $6 \rightarrow \text{Tr}^+$ ) as a function of internal energy for each reactant  $1\text{-}x$  ( $x = o, m$ , and  $p$ ). Results are shown in Figure 3.  $\text{Tr}^+$  was produced very little ( $< 5\%$ ) over the internal energy range 2.0–4.5 eV, whereas  $\text{Bz}^+$  was produced abundantly through all three channels. For each isomeric reactant, the relative abundance of  $\text{Bz}^+$  produced from each channel varied with internal energy. The  $3\text{-}o \rightarrow \text{Bz}^+$  channel was the major path for the *o*-isomer and the  $9 \rightarrow \text{Bz}^+$  channel was the major path for both the *m*- and *p*-isomers. Interestingly, the  $7 \rightarrow \text{Bz}^+$  channel was not the major path for the *m*-isomer because most ( $> 70\%$ ) of  $2\text{-}m$  is converted to both  $2\text{-}p$  and  $2\text{-}o$ . The *p*-isomer mostly yielded  $\text{Bz}^+$  through the  $9 \rightarrow \text{Bz}^+$  channel, indicating that *p*-isomer was hardly isomerized to the *m*-isomer. To see the details of coupling between isomers, we counted how many elementary steps were taken to  $\text{Bz}^+$  by each isomer with an internal energy of 2.5 eV at 298 K. Results are presented in Figure 4. In the case of the *ortho* isomer, only 5% of the reactant yielded  $\text{Bz}^+$  in three steps, which is the minimum number of steps for the  $3\text{-}o \rightarrow \text{Bz}^+$  channel (Figure 4(a)). The average number of steps to  $\text{Bz}^+$  from  $1\text{-}o$  was 18, 25, and 84 for the  $3\text{-}o \rightarrow \text{Bz}^+$ ,  $7 \rightarrow \text{Bz}^+$ , and  $9 \rightarrow \text{Bz}^+$  channel, respectively. Nonetheless, the majority (60%) of the  $1\text{-}o$  passed through the  $3\text{-}o \rightarrow \text{Bz}^+$  channel (Figure 3(a)), suggesting that  $4\text{-}m$  isomerized from  $2\text{-}o$  prefers going back to  $2\text{-}o$  than transforming to  $2\text{-}m$ . As the number of steps increases, the transit time through the exit channels increases. Thus, the overall decay of the reactant  $1\text{-}o$  became multiexponential (see Figure 5).

For the *meta* isomer, in sharp contrast to  $1\text{-}o$ , the reactant  $1\text{-}m$  went through the  $7 \rightarrow \text{Bz}^+$  channel mostly in the beginning with four, six, and eight steps (Figure 4(b)), which resulted in approximately 22% of  $\text{Bz}^+$ . The rest (78%) of  $\text{Bz}^+$  was produced through the  $3\text{-}o \rightarrow \text{Bz}^+$  and  $9 \rightarrow \text{Bz}^+$  channels. The average number of steps to  $\text{Bz}^+$  was 4.5, 17, and 43 for the  $7 \rightarrow \text{Bz}^+$ ,  $3\text{-}o \rightarrow \text{Bz}^+$ , and  $9 \rightarrow \text{Bz}^+$  channel, respectively.

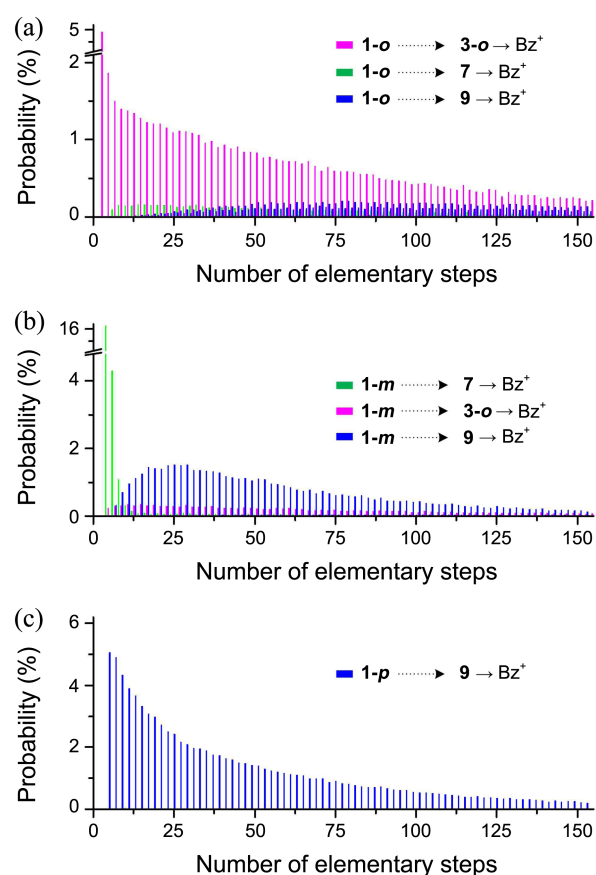


**Figure 4.** The probability of going through  $3\text{-}o \rightarrow \text{Bz}^+$  (magenta),  $7 \rightarrow \text{Bz}^+$  (green), and  $9 \rightarrow \text{Bz}^+$  (blue) to produce  $\text{Bz}^+$  from (a)  $1\text{-}o$ , (b)  $1\text{-}m$ , and (c)  $1\text{-}p$  with the internal energy of 2.5 eV. The number of steps is all odd starting from 3 for  $1\text{-}o$ , all even starting from 4 for  $1\text{-}m$ , and all odd starting from 5 for  $1\text{-}p$ .

These results indicate that  $3\text{-}m$  formed from  $2\text{-}m$  is moving toward the product rather than going back to  $2\text{-}m$  and that  $4\text{-}m$  or  $4\text{-}p$  converted from  $2\text{-}m$  is also moving forward to  $2\text{-}o$  or to  $2\text{-}p$  rather than going backward. The overall decay of the reactant  $1\text{-}m$  was also multiexponential, indicating the fast initial decay followed by the slow steady-state decay (see Figure 5). Unlike  $1\text{-}o$  and  $1\text{-}m$ ,  $1\text{-}p$  resulted in 97% of  $\text{Bz}^+$  through the  $9 \rightarrow \text{Bz}^+$  channel. Nevertheless, on average it took 30 steps to yield the product. This result indicates that the *p*-isomer mostly moves around the *para* path of  $5\text{-}p \leftrightarrow 4\text{-}p \leftrightarrow 2\text{-}p \leftrightarrow 3\text{-}p \leftrightarrow 8 \leftrightarrow 9$  and rarely takes the other paths to the product. As a result, the overall decay of the reactant  $1\text{-}p$  was almost single exponential (see Figure 5).

To further characterize the dissociation kinetics of the chlorotoluene radical cations, we obtained temporal variations of the relative abundances of  $1\text{-}x$  ( $x = o, m$ , and  $p$ ) and  $\text{C}_7\text{H}_7\text{Cl}^+$  with the internal energy of 2.5 eV at 298 K. Results are shown in Figure 5. The relative abundance of  $\text{C}_7\text{H}_7\text{Cl}^+$  decays with the effective time constant ( $\tau_{\text{eff}}$ ) of 10.9, 42.7, and 31.8 ms for the *o*-, *m*-, and *p*-isomers, respectively. The reciprocal of  $\tau_{\text{eff}}$  was used as the overall microcanonical rate constant  $k_{\text{uni}}$  for each isomer. In the case of the *o*-isomer,  $\text{C}_7\text{H}_7\text{Cl}^+$  decays with two time constants (9.02 and 25.6  $\mu\text{s}$ ).

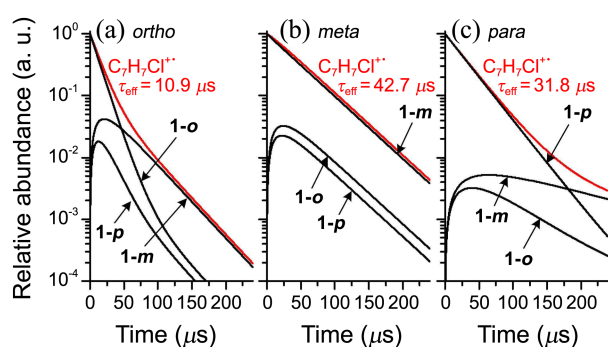


**Figure 5.** Temporal variations of the relative abundances of  $C_7H_7Cl^{+\bullet}$  (red), **1-o**, **1-m**, and **1-p**. Each reactant has the internal energy of 2.5 eV at 298 K at time zero.  $C_7H_7Cl^{+\bullet}$  represents the sum of the reactant and all intermediates. **1-o**, **1-m**, and **1-p** denote the initial reactant as well as the transient species. The fitting parameters for Eq. (2) are ( $c_1 = 0.887$ ,  $\tau_1 = 9.02 \mu\text{s}$ ;  $c_2 = 0.113$ ,  $\tau_2 = 25.6 \mu\text{s}$ ) for *ortho*; ( $c_1 = 0.99$ ,  $\tau_1 = 43.0 \mu\text{s}$ ;  $c_2 = 0.01$ ,  $\tau_2 = 14.6 \mu\text{s}$ ) for *meta*; ( $c_1 = 0.962$ ,  $\tau_1 = 31.1 \mu\text{s}$ ;  $c_2 = 0.026$ ,  $\tau_2 = 42.9 \mu\text{s}$ ;  $c_3 = 0.012$ ,  $\tau_3 = 150 \mu\text{s}$ ) for *para*.

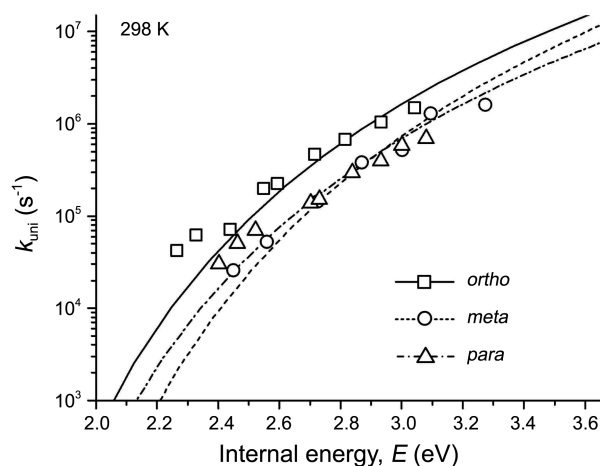


**Figure 6.** The calculated (lines) vs experimental (symbols) rate constants for the unimolecular dissociations of the *o*-, *m*-, and *p*-chlorotoluene radical cations as a function of internal energy. The experimental rate constants are taken from ref. 3.

The fast component is mostly due to the initial decay of **1-o**, whereas the slow component originates from the steady-state decay of  $C_7H_7Cl^{+\bullet}$  after the coupling of **1-o** to both **1-m** and **1-p**. For the *m*-isomer,  $C_7H_7Cl^{+\bullet}$  decays with two time constants (14.6 and 43.0  $\mu\text{s}$ ). The fast component is due to the coupling of **1-m** to both **1-o** and **1-p**, whereas the slow component represents the steady-state decay of all three species (**1-o**, **1-m**, and **1-p**). The effective time constant of 42.7  $\mu\text{s}$  is almost identical to the slow decay time constant. In the case of the *p*-isomer,  $C_7H_7Cl^{+\bullet}$  decays with three time constants (31.1, 42.9, and 150  $\mu\text{s}$ ). However, the coupling is weak and the initial decay is nearly single exponential with the time constant of 31.1  $\mu\text{s}$  similar to the effective time constant of 31.8  $\mu\text{s}$ .

Lastly, we plotted the overall microcanonical rate constants for the unimolecular dissociations of the *o*-, *m*-, and *p*-chlorotoluene radical cations as a function of the internal

energy in Figure 6. Theoretical rate constants are in good agreement with the photoelectron photoion coincidence (PEPICO) experiments.<sup>3</sup> In the internal energy range 2.0–3.6 eV, the *o*-isomer dissociates approximately five times faster than both the *m*- and *p*-isomers. The *m*-isomer is the slowest one in the low energy region but it starts dissociating faster than the *p*-isomer in the high energy region above 2.9 eV. This turn-over is also apparent in the PEPICO data. However, in the low energy region below 2.5 eV, theoretical rate constants deviate from the experimental data for all three isomers. This discrepancy could be due to the uncertainties in the potential energy calculations as well as the radiative cooling of the activated ions, as discussed in our previous report on the coupled unimolecular dissociation kinetics of the bromotoluene radical cations.<sup>13</sup>

## Discussions

According to the recent DFT calculation,<sup>10</sup> there is another path for the production of the benzylium ion. Choe has reported the isomerization of the *o*-chlorotoluene radical cation to the benzyl chloride radical cation *via* Cl migration,<sup>10</sup> similarly to the isomerization from *o*-xylene to the ethylbenzene *via*  $\text{CH}_3$  migration.<sup>17</sup> This benzyl chloride path can yield the benzylium ion by direct C–Cl cleavage; however, the barrier for the Cl migration is much higher than those for H-atom and  $\text{CH}_2$  migrations and the dissociation rate constant for the benzyl chloride path is about two orders of magnitude less than those for the other four paths. Thus, the benzyl chloride path is not included in the present work. Furthermore, the direct C–Cl cleavage from **1-x** to the tolylium ion is also excluded in the present work because the barrier height is estimated to be 75, 77, and 82  $\text{kcal mol}^{-1}$  for the formation of *o*-, *m*-, and *p*-tolylium ions, respectively,<sup>18</sup> which is nearly twice that for **1-x**  $\rightarrow$  **2-x**.

In comparison with our previous work<sup>11</sup> on the unimolecular dissociations of the chlorotoluene radical cations, we changed the level of theory from SCF to DFT with the B3LYP functional. At the SCF level of theory, the transition state for [1,3]  $\alpha$ -H migration (**1-x**  $\leftrightarrow$  **3-x**) is lower in energy than that for [1,2]  $\alpha$ -H migration (**1-x**  $\leftrightarrow$  **2-x**). Thus, the benzylium and tropylium ions are split directly from **1-x** and the **1-x**  $\leftrightarrow$  **2-x** process proceeds far slower than the **1-x**  $\leftrightarrow$  **3-x** process. Consequently, the *o*-, *m*-, and *p*-isomers are considered to be uncoupled and independent of one another. Moreover, the temporal variation of  $C_7H_7Cl^{+\bullet}$  shows a single exponential decay although the multiple-barrier dissociation processes proceed with an induction period. At the DFT level of theory, the transition states for **1-x**  $\leftrightarrow$  **3-x** and **2-x**  $\leftrightarrow$  **3-x** are found to be identical. Therefore, the **1-x**  $\leftrightarrow$  **3-x** process is excluded from the mechanism based on the least action principle<sup>13</sup> and **2-x** is taken as the common intermediate for the low-energy H-atom and methylene migration paths to the product ions.

The extent of coupling depends on the energy levels of **1-x** and **2-x** as well as the internal energy and the reaction time. Because the energy level of **2-x** decreases in order of **2-m**  $>$

$2-o > 2-p$  and that of  $1-x$  also decreases in order of  $1-m \sim 1-o > 1-p$ , the coupling accumulates the most stable  $p$ -isomer. Of the three isomers, the *meta* experiences the largest coupling with the other isomers, whereas the *para* tends to retain its structure. The number of steps taken before dissociation of  $1-x$  suggests that a high-energy portion of the reactant dissociates fast to the benzylium ion without coupling in the beginning. A low-energy portion undergoes multiple isomerization processes prior to the dissociation. Thus, the coupling among three *o*-, *m*-, and *p*-isomers is considered to be a thermodynamically controlled process requiring some induction period, but the overall dissociation of each isomer is a kinetically controlled process. The theoretical rate-energy curve shown in Figure 6 supports this statement. In the low-energy region, the *m*-isomer dissociates more slowly than the *p*-isomer. As the internal energy increases above 3 eV, the *m*-isomer dissociates faster than the *p*-isomer because more of the *p*-isomer goes through slow coupling processes. Without coupling, this crossover of the rate-energy curves of the *m*- and *p*-isomers won't happen, as we have shown in our previous work.<sup>11</sup> This crossover is also apparent in the experimental data and the coupled scheme describes the observed dissociation kinetics better than the uncoupled one.

### Conclusion

The thermodynamic stabilities of the *o*-, *m*-, and *p*-isomers determine the flux to three different dissociation paths to the benzylium ion. In the beginning, each isomer dissociates fast to the product without coupling, but, later on, each reactant dissociates slowly due to the coupling to the other two isomers *via* CH<sub>2</sub> migration, thus showing the steady-state decay. The extent of coupling between isomers is thermodynamically controlled, whereas the product branching ratio (Bz<sup>+</sup>/Tr<sup>+</sup>) is kinetically controlled. With these findings, we conclude that the coupled unimolecular process cannot be described as a single-barrier process with a single exponential decay. The full kinetic simulation is needed to study

the energy- and time-dependent branching of each isomer to the competing dissociation paths. The present result also calls for further experiments to confirm the time- and energy-dependence of branching to each dissociation path.

**Acknowledgments.** J. Seo acknowledges the postdoctoral support from the Brain Korea 21 program administered by the Ministry of Science, ICT, and Future Planning of Korea. And the publication cost of this paper was supported by the Korean Chemical Society.

### References

1. Dunbar, R. C.; Honovich, J. P.; Asamoto, B. *J. Phys. Chem.* **1988**, *92*, 6935.
2. Baer, T.; Morrow, J. C.; Shao, J. D.; Olesik, S. *J. Am. Chem. Soc.* **1988**, *110*, 5633.
3. Olesik, S.; Baer, T.; Morrow, J. C.; Ridal, J. J.; Buschek, J. M.; Holmes, J. L. *Org. Mass Spectrom.* **1989**, *24*, 1008.
4. Choe, J. C.; Kim, M. S. *Int. J. Mass Spectrom. Ion Processes* **1991**, *107*, 103.
5. Shin, S. K.; Han, S. J.; Kim, B. *Int. J. Mass Spectrom. Ion Processes* **1996**, *157/158*, 345.
6. Kim, B.; Shin, S. K. *J. Chem. Phys.* **1997**, *106*, 1411.
7. Kim, B.; Shin, S. K. *J. Phys. Chem. A* **2002**, *106*, 9918.
8. Shin, S. K.; Kim, B.; Jarek, R. L.; Han, S. J. *Bull. Korean Chem. Soc.* **2002**, *23*, 267.
9. Kim, S.-J.; Shin, C.-H.; Shin, S. K. *Mol. Phys.* **2007**, *105*, 2541.
10. Choe, J. C. *J. Phys. Chem. A* **2008**, *112*, 6190.
11. Seo, J.; Seo, H.-I.; Kim, S.-J.; Shin, S. K. *J. Phys. Chem. A* **2008**, *112*, 6877.
12. Choe, J. C. *Int. J. Mass Spectrom.* **2008**, *278*, 50.
13. Seo, J.; Kim, S.-J.; Shin, S. K. *J. Phys. Chem. A* **2013**, *117*, 11924.
14. Frisch, M. J.; Trucks, G. W.; Schlegel, H. B.; Scuseria, G. E.; Robb, M. A.; Cheeseman, J. R.; Montgomery, J. A., Jr.; Vreven, T.; Kudin, K. N.; Burant, J. C. *et al. Gaussian 03*, Revision B.04; Gaussian, Inc.: Pittsburgh, PA, 2003.
15. Sinha, P.; Boesch, S. E.; Gu, C.; Wheeler, R. A.; Wilson, A. K. *J. Phys. Chem. A* **2004**, *108*, 9213.
16. Baer, T.; Hase, W. L. *Unimolecular Reaction Dynamics: Theory and Experiments*; Oxford University Press: New York, 1996.
17. Choe, J. C. *Chem. Phys. Lett.* **2007**, *435*, 39.
18. Shin, S. K. *Chem. Phys. Lett.* **1997**, *280*, 260.